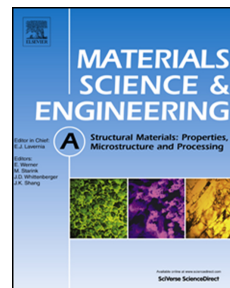


Accepted Manuscript

One-step annealing optimizes strength-ductility tradeoff in pearlitic steel wires

L. Xiang, L.W. Liang, Y.J. Wang, Y. Chen, H.Y. Wang, L.H. Dai



PII: S0921-5093(19)30561-1

DOI: <https://doi.org/10.1016/j.msea.2019.04.086>

Reference: MSA 37836

To appear in: *Materials Science & Engineering A*

Received Date: 11 August 2018

Revised Date: 21 April 2019

Accepted Date: 22 April 2019

Please cite this article as: L. Xiang, L.W. Liang, Y.J. Wang, Y. Chen, H.Y. Wang, L.H. Dai, One-step annealing optimizes strength-ductility tradeoff in pearlitic steel wires, *Materials Science & Engineering A* (2019), doi: <https://doi.org/10.1016/j.msea.2019.04.086>.

This is a PDF file of an unedited manuscript that has been accepted for publication. As a service to our customers we are providing this early version of the manuscript. The manuscript will undergo copyediting, typesetting, and review of the resulting proof before it is published in its final form. Please note that during the production process errors may be discovered which could affect the content, and all legal disclaimers that apply to the journal pertain.

One-step annealing optimizes strength-ductility tradeoff in pearlitic steel wires

L. Xiang^{a,b,c}, L.W. Liang^{a,c}, Y.J. Wang^{a,c}, Y. Chen^{a,c}, H.Y. Wang^{a,c}, L.H. Dai^{a,c*}

^a*State Key Laboratory of Nonlinear Mechanics, Institute of Mechanics, Chinese Academy of Sciences, Beijing 100190, China*

^b*Institute of Systems Engineering, China Academy of Engineering Physics, Mianyang, Sichuan 621999, China*

^c*School of Engineering Science, University of Chinese Academy of Sciences, Beijing 101408, China*

Abstract

In this paper, the mechanical properties of a cold-drawn wire ($\varepsilon = 2.43$) are modulated by simple annealing and the variation of its microstructure is characterized by transmission electron microscopy (TEM), X-ray diffraction (XRD) and molecular dynamics (MD) simulation. The tensile ductility of the wire can be improved for about three times without compromising its strength when being annealed at 325°C for 10-30 min. It is convinced that solid solution of carbon atoms from decomposed cementite lamellae improve the wire strength at low temperature annealing (up to 250°C) and make the wire strength basically equal the as-drawn state even though cementite lamellae are weakened by cementite recrystallization at 325°C. And

*Corresponding author. Tel.: +86 10 82543958; fax: +86 10 82543977.

E-mail address: lhdai@lnm.imech.ac.cn (L.H. Dai).

reversely the weakening cementite layers lead to the great improvement of wire ductility at this time since it relaxes the restriction to the moving of dislocations. At higher annealing temperature, the wire strength decreases with the growth of cementite and ferrite grains. The appearance of nano-recrystallized cementite grains at a medium annealing temperature may be a critical factor governing the enhanced wire mechanical properties.

Keywords: Pearlitic steel wire; carbon state; annealing; strength and ductility; atomistic simulations

1. Introduction

Cold-drawn pearlitic steel wires are widely used as engineering structures such as wire ropes, suspension bridges, springs and automobile tire cords due to their combination of ultrahigh strength and applicable ductility. During the past decades, wires have become the strongest bulk steel products with a strength even up to about 7 GPa [1]. Usually the steel wires are drawn from the hot roll bars, which undergo isothermal transformation of austenite at temperatures of 480-550°C (i.e. patenting) [2, 3]. The steel structure in this case is a fine lamellar pearlite with interlamellar spacing below 100 nm. Then the wires experience a cold-drawn process with severe plastic deformation (SPD) and get their high strength gradually. Great efforts have been made to understand the microstructural evolution and its effect on strength upon cold drawing [4]. Meanwhile in many engineering applications, such as suspension bridges

and power cables, wires are subjected to hot-dip galvanization or blueing to improve their anti-corrosion property [5, 6], so the thermal stability of cold-drawn wires as well as their microstructural mechanisms associated with heat treatment are also widely concerned by researchers.

Generally speaking, one would like to acquire not only strong but also ductile steel wires, since ductility is very important to prevent abrupt failure of wire material under service conditions. However, during the cold-drawn process, wire strength is improved while ductility usually decreases concomitantly. With increasing drawing strain, wire radius and the interlamellar spacing of pearlitic plates decrease, so wire strength increases with the smaller interlamellar spacing (obeying the Hall–Petch relation [7]). But wire ductility drops due to the stronger restraint to dislocations from cementite layers. Some exceptions only happen to wires with a high drawing strain (bigger than 4) [1, 8, 9]. The reason may be on the one hand, the thickness of cementite lamella at this stage can be below 1 nm [8] and thin cementite shows a certain extent of ductility due to size effect [10]. On the other hand, atom probe tomography (APT) results show that the cementite lamellae begin to extensively decompose into pieces under severe plastic deformation (SPD) [1], which may release certain constraint to dislocations and contribute to the ductility of wires. However, the diameter of wires with high drawing strain can be very thin (even below 0.1 mm in [1, 8]), leading to severe limitations for the broad engineering applications.

Heat treatment is another effective method to control wire mechanical property and microstructure. Wire strength has been found to be slightly improved at the low

annealing temperature [6, 11, 12] with the reduction of its ductility [6]. Then the wire strength decreases and the wire ductility is enhanced continuously within higher temperatures, or worse, the wire with an as-drawn strength of 6.35 GPa get a deteriorated ductility with increasing temperature above 350°C [13]. Under low temperature annealing, the wires experience statics train aging and recovery of microstructure, while recrystallization and grain growth of cementite and ferrite appear at higher temperatures [12]. However, the change of microstructure in the low-temperature annealed wires can hardly be observed through TEM [5, 13, 14], even though the strength (especially the yield strength) may have varied apparently. It indicates that more delicate variation has happened in the wire material. Through positron annihilation spectroscopy (PAS), researchers found that at low temperatures up to about 523 K, annihilation of carbon-vacancy complexes (single or perhaps di-vacancies) is probable and carbon might diffuse to grain boundaries, interphase boundaries or dislocations [15, 16]. An interesting APT result exhibits a complete dissolution of cementite with a uniform distribution of carbon over the whole sample is generated after annealing at 423 K, which indicates the decomposition of cementite during low temperature annealing.

It seems that improving the strength and ductility of wires simultaneously is improbable to achieve. Nevertheless, it is find that the tensile strength and ductility of a moderate drawn wire ($\epsilon = 2$) was found to be both improved slightly under low temperature annealing [17, 18]. The strength increase is believed to result from cementite nano-grains decoration of the ferrite dislocations and the enhanced ductility

may originate from defect recovery when the microstructure of steel wires remains to be lamellar. However, possible conditions to achieve a strength-ductility balance are not given in detail explicitly, since their attention were paid to other important topics, like the crystallization of cementite [17] and torsion property of pearlitic wires [18]. To the author's view, the strengthening and plasticity mechanism of cold-drawn pearlitic wires under the annealing process have not yet been totally understood so far.

In recent years, atomistic simulations are employed to help explain the microstructural evolution and mechanical mechanism of the pearlitic wires. With molecular statics (MS), binding energy between a carbon atom and screw or edge dislocations in bcc iron is calculated at the atomic scale. The results show a quantitative agreement with elasticity theory, as long as anisotropic elastic calculations are performed and both the dilatation and the tetragonal distortion induced by the carbon interstitial are considered [19]. A multiscale simulation approach based on atomistic calculations and a discrete diffusion model is developed to explain the mechanism of cementite composition during wire drawing [20]. Results favor the so-called drag mechanism, by which a mobile screw dislocation is able to transport carbon atoms along its glide plane, and show a good agreement with C concentration data in ferrite from APT observation [21]. MD simulations are also carried out to investigate the misfit dislocations at ferrite/cementite interfaces and for various orientation relationships (ORs) and the most probable ORs in pearlitic steel is given [22]. By means of aberration-corrected TEM imaging and density functional theory (DFT), it is found that the interface with terminating layer Fe–C–Fe in

cementite has the lowest energy due to the formation of interfacial Fe–C bonds [23].

In this paper, different microstructure and mechanical properties of cold-drawn wires are obtained by annealing at temperatures between 175 and 475 °C. The TEM and XRD techniques are taken to characterize the evolution of microstructure in wire material. MD simulations are conducted to elucidate the interaction between carbons and dislocations, and the plastic mechanism of the annealed pearlitic wire. Then the strengthening and plasticity mechanism with relation to the transformation of carbon state are analyzed via consistent views from both experimental characterization and atomic-scale observation from MD. Finally, the probable annealing condition to improve both the wire strength and ductility is discussed.

2. Methodology

2.1 Experimental procedures

The studied material is from drawn pearlitic steel wires with a near-eutectoid content of Fe-0.72C-0.51Mn-0.24Si wt.%. Steel rods were quenched in salt bath at about 550°C after being fully austenized at 900°C, and completed isothermal pearlitic transformation. Then the patented wires were drawn from a diameter of 2.90 mm to 0.90 mm. The reduction corresponds to a true drawing strain of 2.34 when applying the equation:

$$\varepsilon = 2 \ln(d_0 / d)$$

(1)

where d_0 is the initial wire diameter and d is that of the drawn wire. The drawing process is carefully controlled and the wires were wet-lubricant to avoid distinct temperature rise during deformation.

Post-drawing annealing was conducted at an interval of 75°C increments from 175°C to 475°C. The wires were put in glass tubes with vacuum to avoid surface oxidation and followed by air cooling to room temperature. The tensile tests were performed on wires of all annealing levels on an MTS 810-100 kN servo-hydraulic testing machine with a loading rate of 2 mm/min.

Fracture surfaces of tensioned wires were examined by a scanning electron microscope (SEM, JEOL, JSM-7100F). Internal microstructures were studied by TEM using a JEOL JEM-2100F instrument operated at 200 kV. Thin films for TEM observation were cut from the center of the wires along the longitudinal direction, which were first mechanically ground to ~50 μm thickness and then thinned by a twin-jet polishing method in a solution of 5% perchloric acid in ethyl alcohol with a voltage of 40V at 20°C.

The phases of the samples were examined by XRD in a Rigaku SmartLab 9 diffractometer using Cu K α radiation. The analysis of the dislocation density of the pearlitic steel wires was based on the modified Williamson-Hall method, in which an increase in line broadening with increasing diffraction order is explained as strain anisotropy caused by dislocations. The modified Williamson-Hall equation is expressed as follows:

$$\Delta K = 1/D + \sqrt{\pi B^2 b^2} \cdot \sqrt{\rho} (KC^{1/2}) + O\left((KC^{1/2})^2\right)$$

(2)

where $K=2\sin(\theta/2)/\lambda$ and $\Delta K=\Delta\theta \cdot \cos(\theta/2)/\lambda$. In Eq. (2), θ and $\Delta\theta$ are diffraction angle and the full width at half maximum (FWHM) for every diffraction peak respectively; ρ and b are the dislocation density and the Burgers vector, respectively; D is the average grain size, B is a parameter depending on the outer cut-off radius of the dislocations; and O stands for a higher-order term $KC^{1/2}$. The variable C is a dislocation contrast factor that depends on the relative orientations between the Burgers and line vectors of dislocations and the diffraction vector. A detailed procedure to determine C is given in [24]. A detailed process to calculate the density in pearlitic wires via the modified Williamson-Hall can be seen in [25-27].

2.2 MD simulations

Microstructure of pearlite consists of alternating lamellae of ferrite (α -Fe, BCC) and nanoscale orthorhombic cementite (Fe_3C). Although a variety of orientation relationships have been reported over the past years, the Bagaryatsky orientation relationship [28] has a high degree of registry and appears to be the most energetically stable interface to form between ferrite and cementite [29, 30], which is adopted in the present model setup. The Bagaryatsky orientation relationship is most commonly observed as follows:

$$[100]_{\text{cem}} \parallel [1\bar{1}0]_{\text{fer}}$$

$$[010]_{\text{cem}} \parallel [110]_{\text{fer}}$$

$$(100)_{\text{cem}} \parallel (11\bar{2})_{\text{fer}}$$

the subscripts “cem” and “fer” in this paper denote cementite and ferrite, respectively. Four different models (Fig. 1) which comprise of bulk ferrite and bulk cementite were established. The simulated models have the brick shape, with dimensions about $L_x \times L_y \times L_z = 52.6 \times 15.5 \times 44.9 \text{ nm}^3$ (~2.5 million atoms), oriented along the principal x : $[1\bar{1}0]$, y : $[111]$ and z : $[\bar{1}\bar{1}2]$ axes of the ferrite phase, respectively. Six repeats of each lattice in normal direction have been confirmed to be sufficient to eliminate the effects of free surface on the calculated interfacial energies [29]. Therefore, the layer thickness of ferrite, cementite, ferrite (with dislocations), and vacuum (from bottom to up in Fig. 1) are approximately 153.6 Å, 40.0 Å, 154.1 Å, and 100.0 Å in the z -axis direction, respectively. To mimic the experimental conditions, we introduce pre-existing dislocation density in the ferrite with a loading-unloading technique, with uniaxial tensile elongation up to tension strain of 30%. Such operation can avoid the artificial interface plasticity with different mechanism of dislocation nucleation from the ferrite-cementite interface.

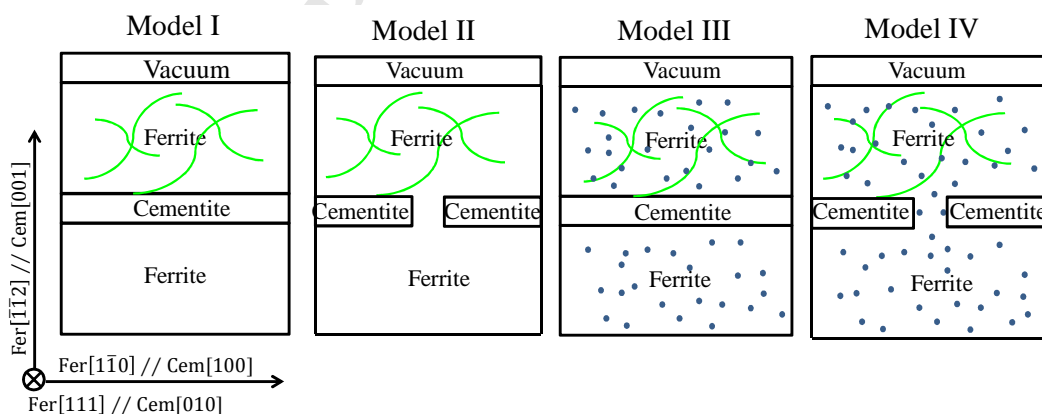


Fig. 1. Schematic demonstration of the four different atomistic models. Model I and III have continuous layer of cementite, while Model II and IV have non-continuous cementite layer. The

carbon concentration in ferrite in Model III and IV is about 0.37 at. %. The ferrite layer above cementite has pre-existing dislocations. Green curves correspond to dislocations. Blue particles represent carbon atoms.

MD simulations are performed with the package Large-scale Atomic/Molecular Massively Parallel Simulator (LAMMPS) [31]. The atomistic interaction is modeled by the modified embedded-atom method (MEAM) [32] which predicts more reliable lattice parameters and energetics over the embedded-atom method (EAM) [33] although the former is more expensive. Table 1 shows the lattice constants and interfacial energy calculated by the MEAM potential for cementite and ferrite. The calculated values of the lattice constants of both phases are in good agreement with experimental data [28] and that of other calculations [29].

In order to generate dislocation in ferrite, we first constructed a bulk ferrite with perfect lattice of approximately one million atoms in a slab of dimensions of $L_x \times L_y \times L_z = 41.1 \times 16.8 \times 18.2 \text{ nm}^3$. Periodic boundary condition was applied in each direction. Energy minimization was performed by using the conjugate gradient algorithm, followed by a thorough relaxation of the stress tensor. Simulated structure was then thermally equilibrated for 200 ps at 300 K and loaded along x-axis to the tensile strain of $\varepsilon = 0.30$ after yielding, with a prototypical MD strain rate of 10^8 s^{-1} . After that, the ferrite was compressed along x-axis to the stress condition of $\sigma_x = 0.00 \text{ GPa}$ under the same strain rate. The ferrite model with dislocation was then thermally equilibrated again for 80 ps at 300 K. Finally, the dislocated ferrite was cooled to 0.2 K within 80 ps. The generated dislocation density in ferrite is about

$4.63 \times 10^{16} \text{ m}^{-2}$. The isothermal stress relaxation in this work was achieved by Nosé-Hoover thermostat [34, 35], and the stress tensor was controlled by a Parrinello-Rahman technique [36] within a NPT ensemble, where N , P and T denote number of atoms, pressure and temperature, respectively. For the carbon concentration, atom probe tomography (APT) studies probing perpendicular to the drawing axis found that carbon concentration in ferrite is $c_c = 0.25$ at. % (0.054 wt. %) when a wire is drawn to a true strain magnitude of $\varepsilon = 2.0$; $c_c \approx 0.6$ at. % (0.13 wt. %) for the case of $\varepsilon = 3.47$, $\varepsilon = 5.0$, corroborating saturation of cementite dissolution [37, 38]. Considering both the experimental results and the modeling convenience, the addition of carbon atoms with concentration of $c_c = 0.37$ at. % was applied for the present models. The random positions of carbon atoms was constructed by the software PACKMOL [39].

In the tensile test along x-axis, a three-dimensional periodic boundary condition was applied and the MD timestep was chosen as 2 fs. After setup of the atomistic models (as shown in Fig. 1), energy minimization was performed at 0 K by using the conjugate gradient algorithm to relax the interface stress, followed by the relaxation of the stress tensor of the whole interface model. The models were then thermally equilibrated for 200 ps at 300 K. Uniaxial tensile loading was performed along the ferrite $[1\bar{1}0]$ direction (axis L_x) with a constant strain rate of 10^8 s^{-1} , while the stress along the ferrite $[111]$ direction (axis L_y) was relaxed to stress-free condition and the dimension of L_z was kept unchanged to maintain the vacuum layer. The software OVITO [40] was used to visualize the defects in the interface models. We use

dislocation extraction algorithm (DXA) [41] to recognize dislocations and their characteristics.

3. Experimental results

3.1. Tensile test

Engineering stress-strain curves for the wires annealed at different annealing temperature for 10 min are shown in Fig. 2a, together with the curve for the initial drawn wire. The mechanical properties are determined by using a standardized tensile test method and results are given in Figs. 2b and c. The strength (especially the yield stress) is enhanced significantly when annealing at 175 °C and then decreases gradually with the rise of temperature. Compared with the as-drawn wires, the tensile strength is improved when the treatment temperature rises up to 325 °C. The variation of wire ductility roughly shows an opposite trend in contrast to the strength, i.e. the stronger wire has a smaller elongation, compared to the as-drawn state. However, an exceptional but interesting point comes out when the wires are treated at 325 °C. The ductility of the wires is much larger than that of the initial wires, but contrary to what one might suppose, the strength is not cut down but slightly increased instead.

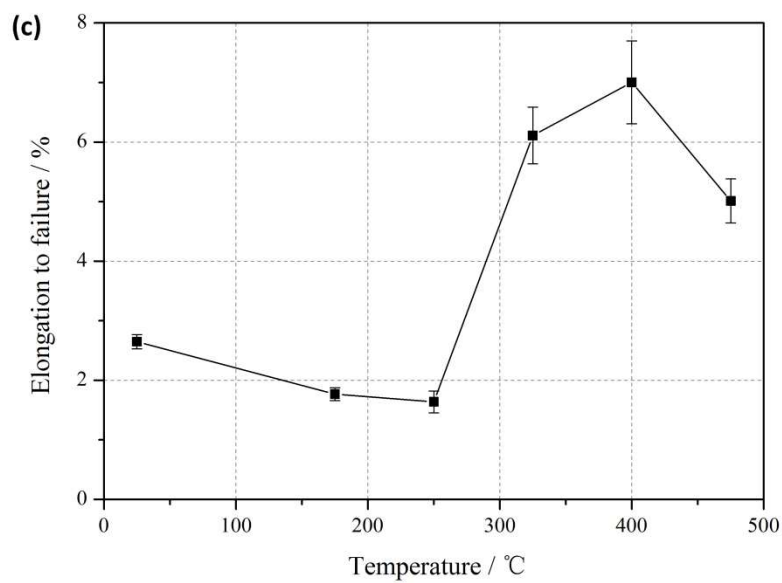
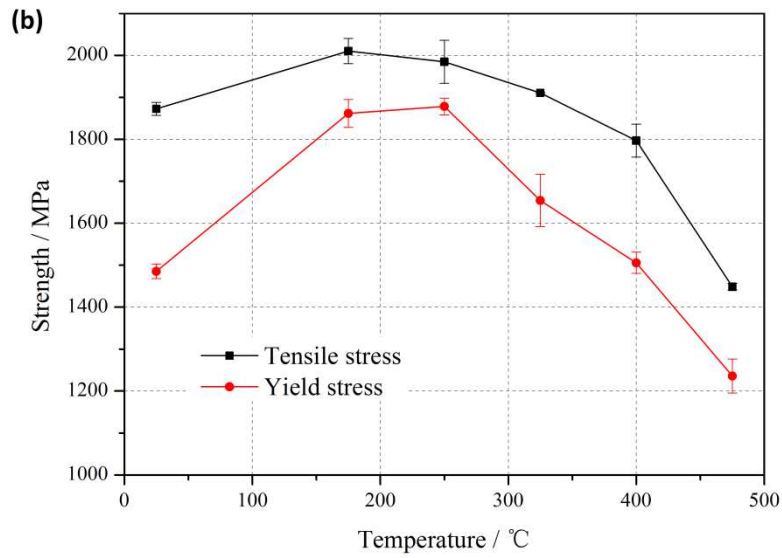
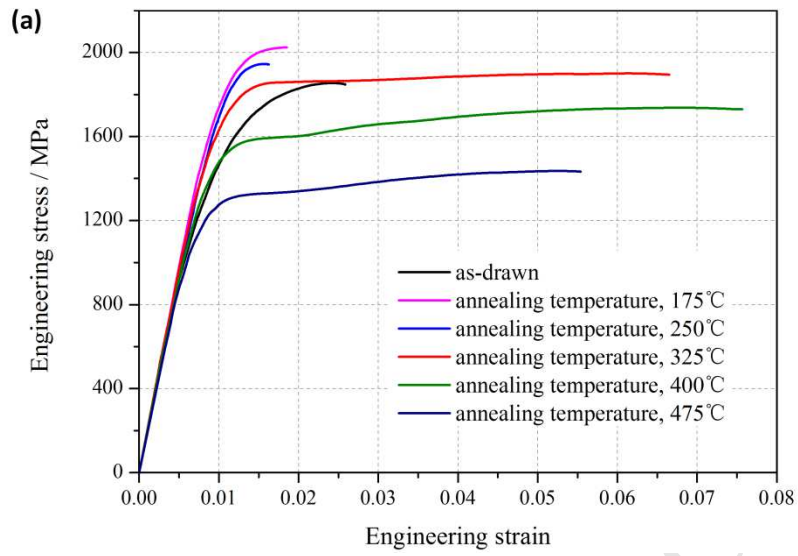


Fig. 2. (a) Engineering tensile stress–strain curves of the annealed wires at different annealing temperatures for 10 min. (b) Ultimate tensile stress and 0.2% yield stress vs. annealing temperature. 0.2% Yield stress. (c) Influence of annealing temperature on the elongation to failure derived from stress-strain curves shown in (a).

Fig. 3 gives the engineering stress-strain curves for the wires under different annealing time at 325°C. Similar to the results in Fig. 2, strengths of the wires are improved firstly and then decreases with increasing treatment time. Inspiringly, greatly enhanced ductility of the wires can hold for a long time (from about 2 min to 30 min) without losing their strengths. When annealed at 325°C for 30 min, the total elongation is almost increased up to three times as that of the as-drawn wire. This phenomenon is intriguing for making both strong and ductile pearlitic steel wires, as the heat treatment technique adopted here is rather easy to operate.

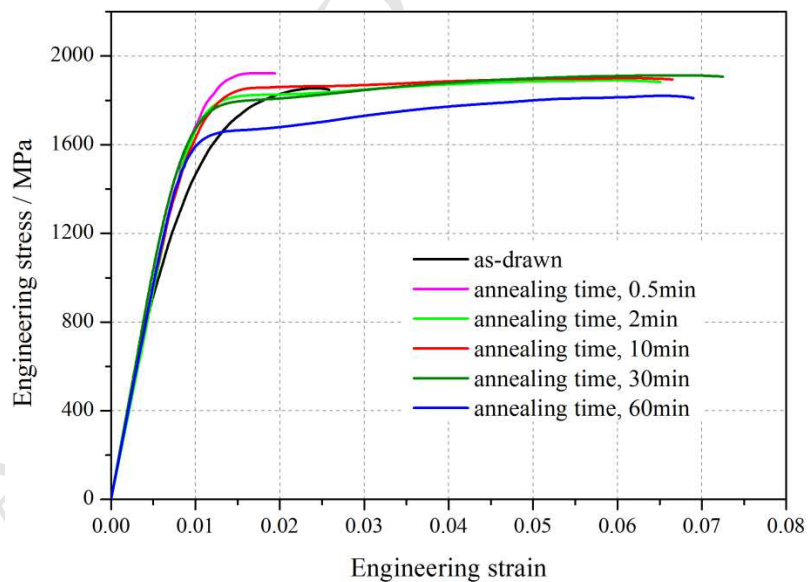


Fig. 3. Engineering tensile stress–strain curves of the annealed wires under different annealing time at 325°C.

3.2. TEM and SEM observations

Fig. 4 illustrates the pearlite lamellae at most area of wires before annealing, where the lamella direction is along with the wire axis. The average interlamellar spacing is about 60 nm and the thickness of the cementite layer is about 6 nm. As the wires undergo severe plastic deformation during the drawing process, plenty of dislocations have accumulated in the ferrite layers.

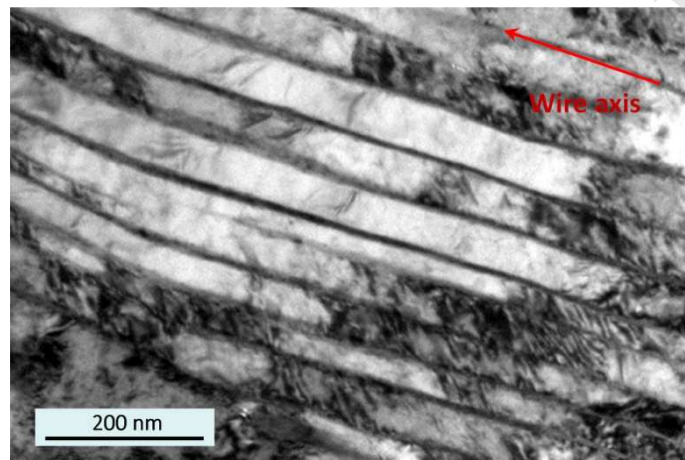


Fig. 4. Microstructure of the as-drawn steel wire observed by TEM.

The microstructures of wires with different annealing temperatures are given in Fig. 5. The annealed wire under 250°C for 10 min shows similar TEM microscopic images with the as-drawn state. The cementite lamellae mostly keep integrated and dislocations still remain in many regions of ferrite. No spherical cementite is found in wire material at this state. When the temperature rises up to 325°C, cementite particles have come out along cementite layers and their size is just about several nanometers (less than the thickness of the remained cementite layer). Subsequently recrystallization grains of cementite grow up to beyond 10 nm with annealing temperature reaching 400°C (Figs. 5c) and the cementite layers begin to be discontinuous and fragmented. In the wires treated at 475°C, many spherical

cementite grains scatter over the inner material and cementite layers have almost disappeared. A selected cementite grain is shown in Fig. 6a and the grain size of the spheroidized cementite has been close to ~ 100 nm at this moment. Stacking faults are observed within the grain, which are probably inherited from the cementite that remained after cold drawing [42]. HRTEM image of the cementite grain and the corresponding selected area diffraction (SAD) pattern along $[001]_{\text{cem}}$ zone axis is given in Fig. 6b, which shows a regular Fe_3C crystalline structure according to the discussion in [43].

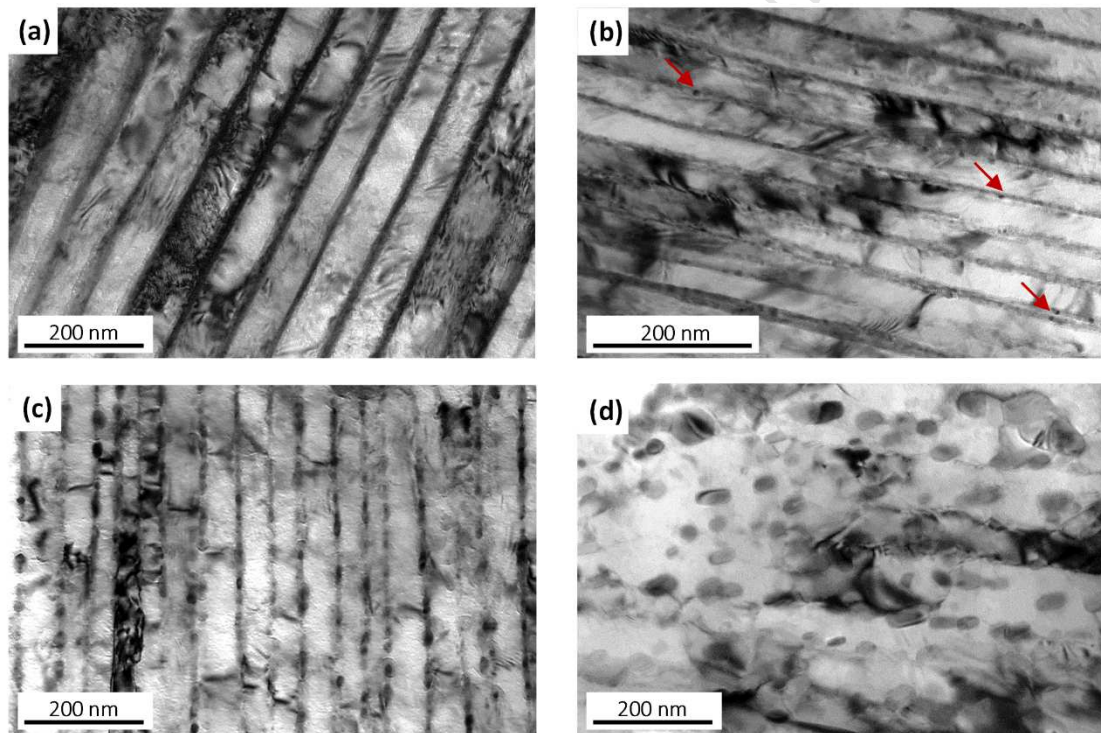


Fig. 5. TEM images showing microstructures of wires after annealing for 30 min at (a) 250°C , (b) 325°C , (c) 400°C , and (d) 475°C . The appearance of the nanoscale spheroidized cementite particles are indicated by arrows in (b).

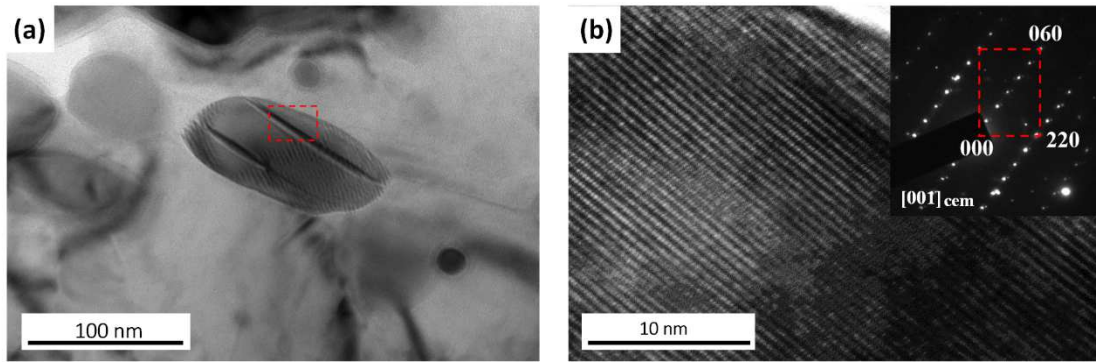


Fig. 6. (a) TEM observation of a nanoscale recrystallized cementite grain in a wire annealed at 475°C for 30 min; (b) HRTEM image of the marked block in (a) and the corresponding SAD pattern.

Fig. 7 shows SEM micrographs of the fracture surfaces of the wires annealed at different temperature for 10 min. All wires exhibit clearly necking and cup-and-cone fracture surfaces. For as-drawn and 250°C 10min annealing wires, there are visible cracks in the low-revolution views. These cracks can be generated where local stress concentrates, namely at ferrite-cementite boundaries, and lead to a relatively lower elongation for wires. When temperature rises up to 325°C, distinct crack disappears and the fracture surface mostly shows a dimple structure. This may be due to the weakening of ferrite-cementite boundaries, since the recrystallization of cementite starts to appear along the cementite layers (Fig. 5b). Therefore wires annealed at 400°C 10 min shows the best ductility as the cementite layers are totally fragmented into pieces (Fig. 5c). For higher annealing temperature (475°C), micro-cracks reappear at the wire fracture surface accompanying the drop of the elongation. As the cementite grains grow up (Fig. 5d), dislocations seem to pin at the boundary of spheroidized cementite, leading to local stress concentration and the initiation of cracks.

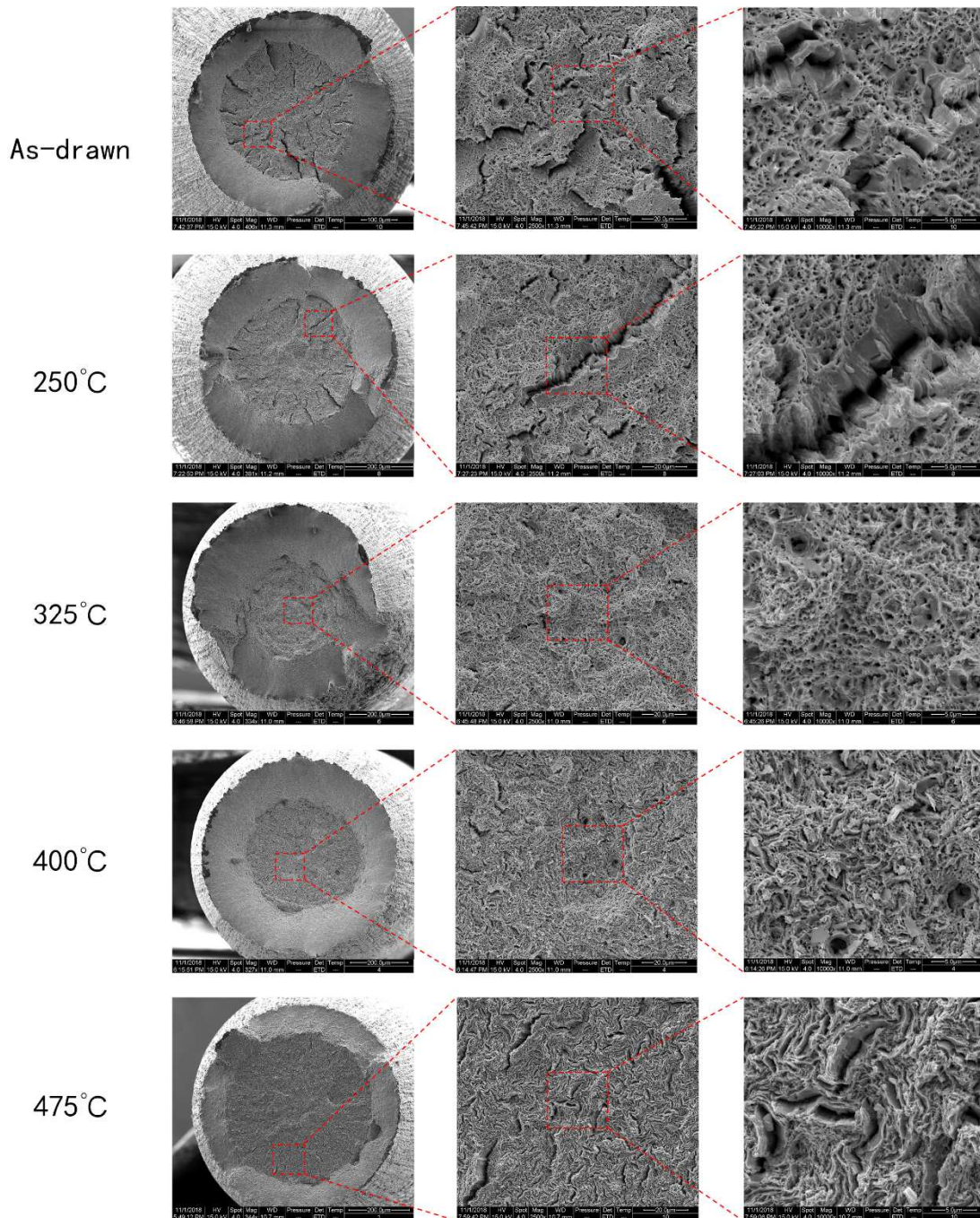


Fig. 7. SEM micrographs of the fracture surfaces of the wires annealed at different annealing temperature for 10 min.

Fig. 8 shows the internal morphology of wires under different annealing time at 325°C. Fig. 8a gives another photograph of wire treated at 325°C for 10 min. The initial recrystallized cementite particles can be clearly observed, whose size is just about several nanometers and less than the thickness of the remained cementite layer.

As being annealed for 30 min (Fig. 8b), the grains of the spherical cementite becomes a little bigger (~ 10 nm). When the annealing time rises up to 60 min (Fig. 8c), the size of cementite has reached tens of nanometers and the previous cementite layers have become disconnected.

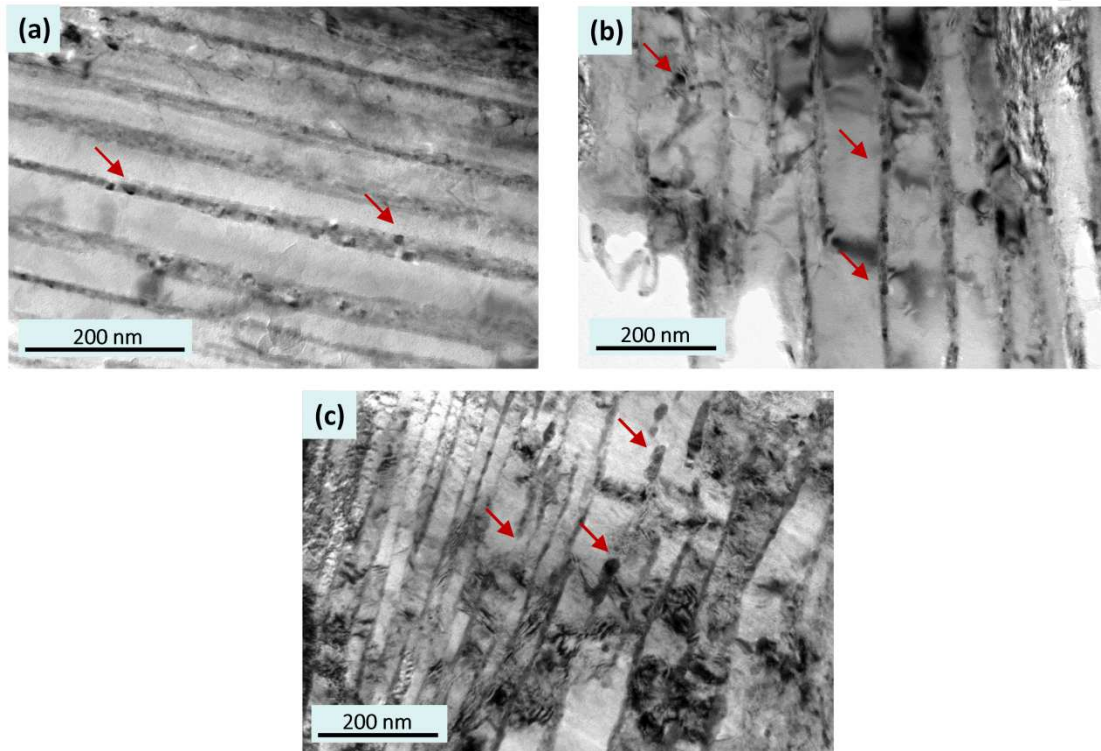
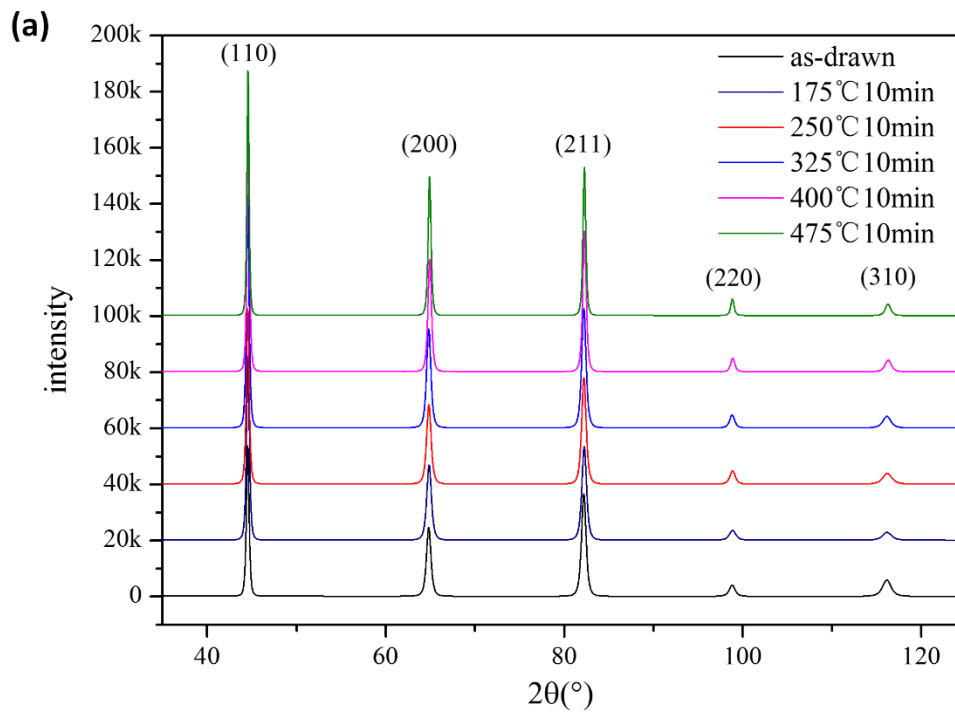


Fig. 8. Microstructures of wires after annealing at 325°C for (a) 10 min, (b) 30 min, (c) 60 min, observed by TEM. Globular cementite grains are marked by arrows.

3.3. XRD analyses

Fig. 9a shows the XRD patterns of the as-drawn and heat-treated steel wires and the truncated strong (110) diffraction peak of the ferrite and the positions of the weak reflections corresponding to the cementite are shown in Fig. 9b. Most cementite peaks of the as-drawn specimen hardly can be seen due to the cementite decomposition

during the severe plastic deformation of the cold-drawn process. Some of the cementite peaks start to appear when the specimen is heat-treated at 325 °C for 10 min, which is consistent with the nano-particles of recrystallized cementite in Figs. 5b and 8a. As the temperature rises, the cementite peaks are more and more distinct, implying the grow-up of cementite grains.



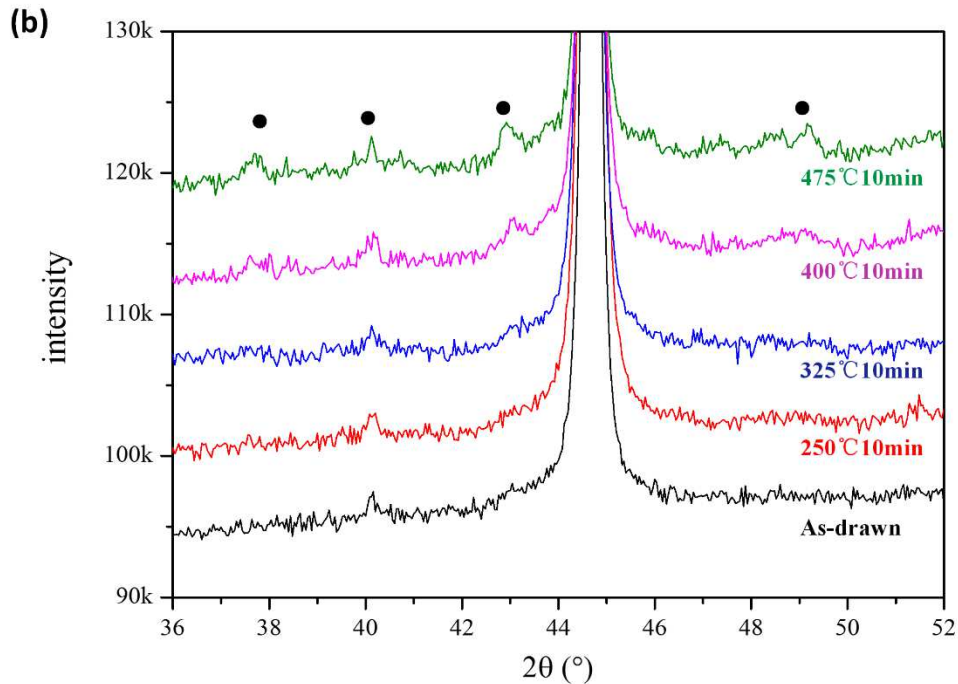


Fig. 9. (a) XRD patterns of the longitudinal cross-sections of the as-drawn specimen and wires heat-treated at different temperatures for 10 min; (b) Truncated strong (110) diffraction peak of the ferrite and diffraction peaks denoted by filled black circles are from cementite phase.

Fig. 10a gives the modified Williamson-Hall plots for the diffraction profiles measured in the as-drawn wires and wires treated at 325°C 10min and 475°C 10min. It can be seen that the slopes of the modified Williamson-Hall plots decrease with increasing annealing temperature, which indicate a decrease of dislocation density upon annealing. Fig. 10b gives dislocation results of the heat-treated wires. It can be seen that the dislocation density of the as-drawn wire reaches the order of 10^{15} m^{-2} . The dislocation density of the heat-treated wires decreases slightly when temperature is less than or equal to 325°C and the annihilation of dislocation accelerates distinctly with higher temperature. Overall the recovery of dislocation happens and the dislocation strengthening to pearlitic wires is reduced during the annealing process. The variation tendency of the dislocation density we get is consistent with the results

in [26, 27].

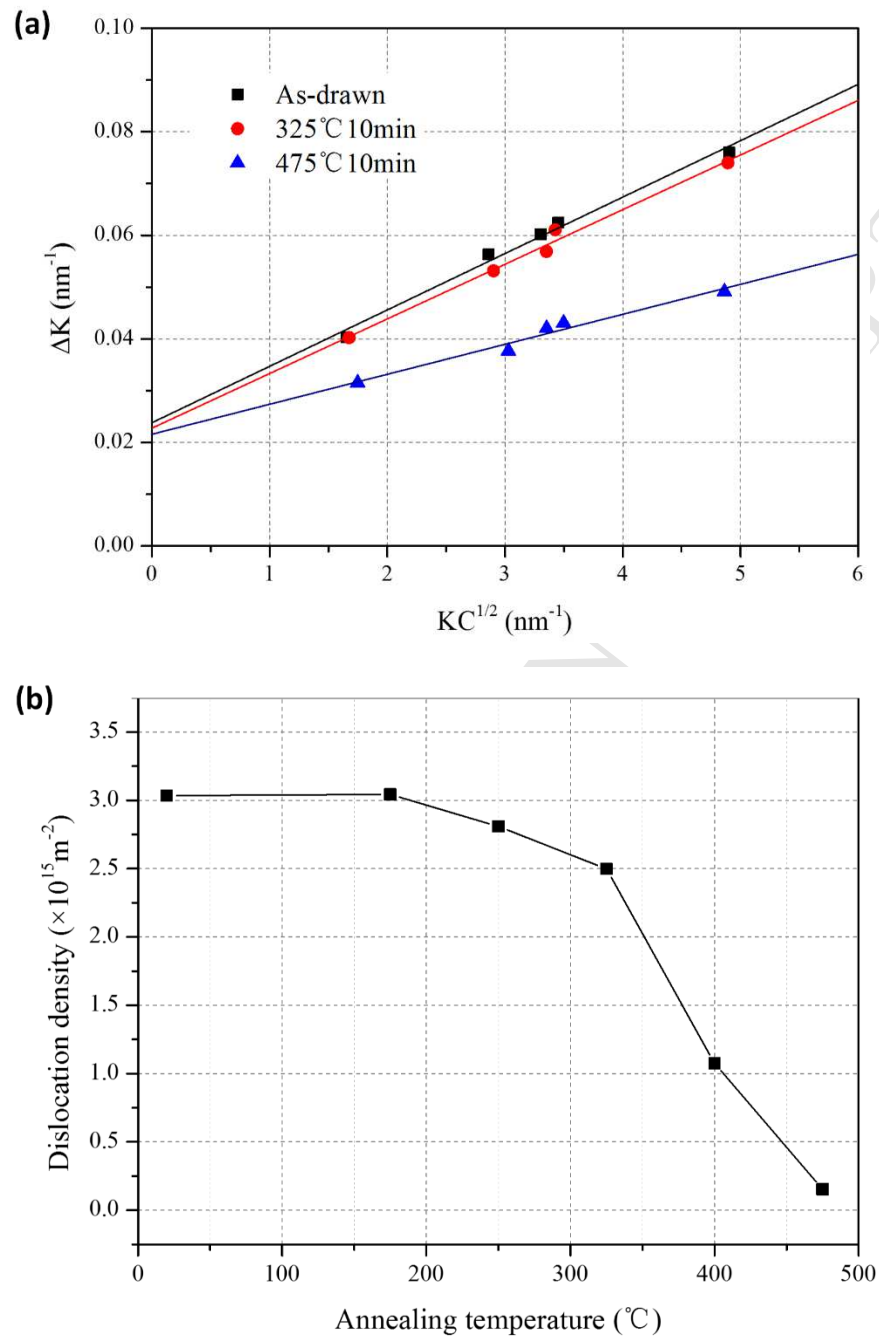


Fig. 10. (a) The modified Williamson-Hall plots for wires treated at different annealing temperature; (b) Dislocation density obtained from modified Williamson-Hall method.

4. Discussion

4.1. Strength and ductility mechanism of pearlitic wires

As is well-known, pearlitic steel wires get their high strength through the severe cold-drawn process [4]. Three mechanisms contributing to the wire strength have been proposed [7, 8]: boundary strengthening σ_b (the strengthening by grain boundaries is replaced by strengthening due to cementite lamellae), dislocation strengthening σ_ρ and solid solution hardening σ_{ss} . Boundary strengthening obeys the classical Hall-Petch relation

$$\sigma_b = k(\varepsilon)(2\lambda)^{-0.5} \quad (3)$$

where λ is the average thickness of the ferrite layers and $k(\varepsilon)$ is a strain dependent parameter. Dislocation strengthening is considered on the assumption of forest or Taylor strengthening and related to the high dislocation density generated from the severe plastic cold-drawn deformation

$$\sigma_\rho = M\alpha\mu b\sqrt{\rho} \quad (4)$$

where M is the orientation factor, α is a constant, μ is the shear modulus of ferrite, b is the Burgers vector and ρ is the dislocation density in the ferrite layer. Solid solution hardening is resulted to the carbon concentration in the ferrite lamellae as cementite decomposition has been proved to be a prevalent phenomenon during the cold-drawn process.

So the strength of the wires can be expressed as

$$\sigma(\varepsilon) = \sigma_0 + \sigma_b + \sigma_\rho + \sigma_{ss}$$

(5)

where $\sigma(\varepsilon)$ is the flow stress at a given drawing strain and σ_0 is the friction stress of the pure ferrite. Among the three mechanisms, the boundary strengthening is considered to be the dominant one contributing to the wire strength [4].

When being annealed at low temperatures (175°C and 250°C), the strengths of wires are higher than that of the as-drawn specimen. However, there is not a distinct difference between the microstructures of the heat treated and as-drawn samples under TEM observation. The pearlite lamella still keeps integrated and no recrystallization of cementite is seen along the cementite layers (Fig. 5a). This indicates that the effect of boundary strengthening is mainly unchanged. At the same time, the effect of dislocation strengthening cannot be enhanced since the dislocation density is slightly reduced. So the increasing of the wire strength most probably results from the solid solution hardening function. It is found through 3DAP technique that cementite in pearlitic steel wires may decompose under low temperature annealing [11, 44]. During the cold-drawn process, the cementite layer can dissolve into fragmentation or even turn to amorphization by dislocations cutting cementite and dragging carbon along the ferrite-cementite interfaces [21, 45]. When the wires are heated, the partly dissolved cementite lose their stability and the carbon atoms can be attracted by the dislocations in the ferrite layers, since the binding energy of carbon to dislocations is greater than that to cementite [46]. The decomposed carbon atoms in ferrite can pin the dislocations and restrain their movement, which leads to the rapid increasing of the yield stresses of wires annealed at 175°C. MD simulation results in Section 4.2 has proved this solid solution hardening mechanism by considering the interaction

between dislocations and carbon atoms. Meanwhile, it is well known that the plastic deformation of metal is mostly involved with the morphology of dislocation. Since dislocations in ferrite have been locked by carbon atoms, a lower ductility for wires annealed at low temperatures (175°C and 250°C) is reasonable.

As the annealing temperature rises to 325°C, the ductility of wires is improved significantly compared with the as-drawn specimens. The cementite recrystallization starts to appear in the cementite layers of the wires at 325°C for 10 min (Figs. 5b and 8a). Fig. 11b gives a HRTEM image of a selected region in Fig. 11a, including a section of cementite lamella and a cementite nano-recrystallization grain. From the FFT images of the selected area in Fig. 11b, the location near the cementite nanograin along the cementite lamella shows the same lattice structure with the adjacent ferrite. It seems that as carbon atoms in some places of cementite layers are attracted to participate in the spheroidization of cementite, the initial cementite lamellae nearby have transformed into ferrite due to the lack of carbon atoms. This means the two separated neighboring ferrite layers become interconnected now, which leads to a bigger free path of dislocations that allow dislocation penetration and a higher ductility of the wires consequently. Meanwhile, the unconnected cementite layers weaken the restriction to dislocations, so that the boundary strengthening effect is reduced and the strengths of wires begin to decrease gradually.

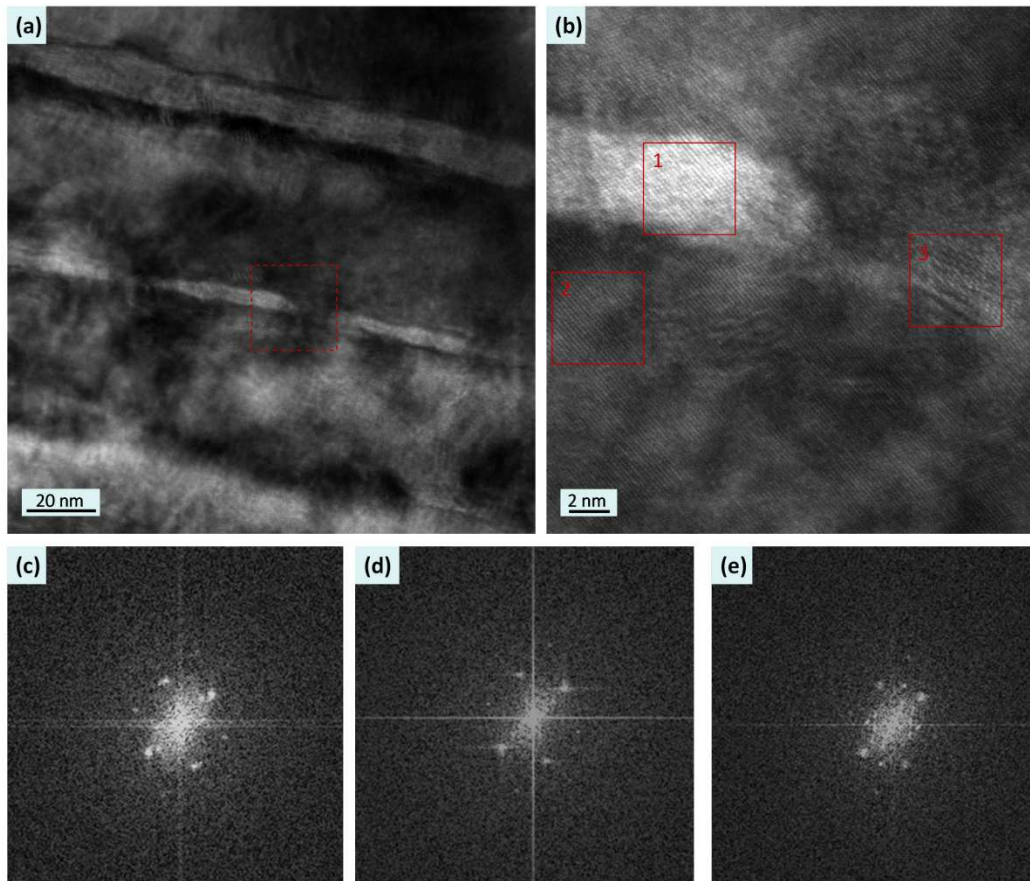


Fig. 11. (a) TEM observation of pearlite lamellae in a wire annealed at 325°C for 10 min. (b) HRTEM image of the marked area in (a), including a cementite nano-recrystallization grain labeled as block '3'. (c-e) FFT patterns of the marked blocks '1', '2' and '3' in (b), respectively.

When the temperature goes up to 400°C, the cementite lamellae have turned into pieces with a greater extent (Fig. 5c), so the strength of wire decreases and ductility increases continuously. The recovery of dislocations in ferrite begins to weaken dislocation strengthening. Also, carbon atoms are participating in the recrystallization process, so the concentration of carbon in ferrite also reduces, which releases the locking of dislocations in ferrite and the decrease of carbon in ferrite enhances the ductility of wires. However, the samples under 475°C reversely have a lower ductility than those in 325°C and 400°C. This may be due to the grain and sub-grain

boundaries generated with the coarsening of ferrite and cementite grains (Fig. 5d), which restrain the movement of dislocations. The wire strength drops concomitantly with the growth of cementite and ferrite grains.

4.2 Atomistic insights into strength and plasticity

Interfacial energy was calculated on the Bagaryatsky orientation relationship to ensure the robustness of the simulations results. The interfacial energy of the system was calculated following the equation [29] :

$$E_{\text{int}} = \frac{E_{\text{total}} - E_{\text{BCC}} - E_{\text{Fe}_3\text{C}}}{L_x L_y} - \gamma_{\text{BCC}} - \gamma_{\text{Fe}_3\text{C}} \quad (6)$$

where L_x and L_y are the dimensions of the interface along x and y directions, and γ_{BCC} and $\gamma_{\text{Fe}_3\text{C}}$ are the surface energies of ferrite and cementite per unit area in the normal dimensions. E_{total} , E_{BCC} and $E_{\text{Fe}_3\text{C}}$ are the total energy of ferrite/cementite system, the bulk energies of bcc Fe and Fe_3C crystal, respectively. To make results more accurate, we use multiple interatomic potentials for the Fe-C system. We predict a series of interfacial energy by using the MEAM, Tersoff [47] and EAM [33] potentials, which are in good agreement with those of predicted by Guziewski et al. [29], as shown in Table 1.

Table 1

Comparison of the lattice constants and interfacial energy of cementite and ferrite by using different potentials with experimental data and that of other calculations.

		MEAM		Tersoff		EAM		Experimental [28]
		This work	Ref.[29]	This work	Ref.[29]	This work	Ref.[29]	
Cementite	a (Å)	4.47	4.47	4.48	4.47	4.84	4.84	4.52
	b (Å)	5.09	5.09	4.96	5.07	4.41	4.41	5.08
	c (Å)	6.67	6.67	6.47	6.45	6.50	6.66	6.73
Ferrite	a (Å)	2.85	2.85	2.89	2.86	2.86	2.87	2.87
Interfacial energy	(J/m ²)	1.01	1.12	0.99	1.03	1.44	1.47	–

The strength and ductility of Fe-C structure should depend on the interaction between dislocation and interface, as well as carbon atom distribution in ferrite. In order to explore the interaction between dislocation and the ferrite/cementite interface, nanoscale continuous cementite and non-continuous cementite layers were constructed, as shown in Fig. 1. Besides, pre-existing dislocations were introduced to the top ferrite layers by loading and unloading technique, while the ferrite layer at bottom had no defects before loading (Fig. 1 Model I and II). The decomposition of cementite leads to transfer of carbon atoms from cementite to ferrite. The addition of carbon diffuses into the bcc Fe lattice in the direction of the two nearest neighbor Fe atoms around the carbon interstitial. Lattice distortion increases the resistance to dislocation, making slip difficult to perform. The ferrite inserted with carbon atoms randomly was constructed to investigate the interaction between carbon atoms and dislocations (Fig. 1 Model III and IV).

The solid solution effect of carbon atom can improve the strength of the pearlite

steel by blocking the motion of dislocation. Fig. 12a and b show the stress-strain curves of the four different models, and Fig. 12c shows the calculated flow stresses of each model under uniaxial tensile loading. The flow stress was determined after yielding statistically. With strain increasing, all curves share a common feature, namely stress drops after peak stress, which corresponds to the dislocation nucleation from the interface. However, the dislocation nucleation behavior is out of our discussion in the present work. Here we concentrate on the behavior of dislocation in the four structures after yielding. The models with carbon atoms in ferrite have a higher flow stress compared with those of models without carbon atoms in ferrite (as illustrated in Fig. 12c). Besides, Fig. 13 shows the interaction between dislocations and carbon atoms during plastic flow. Carbon atoms located on dislocations are observed, which illustrated carbon atoms can block the movement of dislocation and the material has a higher strength. This is expected to be the solid solution strengthening mechanism why strength is increased after annealing. Furthermore, dislocations are observed to be more difficult to spread in Model III or IV than that of Model I or II in supplemental videos along the snapshots of Fig. 14. Interestingly, the models with carbon atoms in ferrite layer have a lower peak stress than those of models without carbon atoms in ferrite layer in Fig. 12a and b. This suggests that new dislocations are easier to nucleate in pearlite with ferrite inserted carbon atoms, namely defects like carbon atoms in ferrite layer may promote the formation of dislocations since point defect reduces the nucleation barriers.

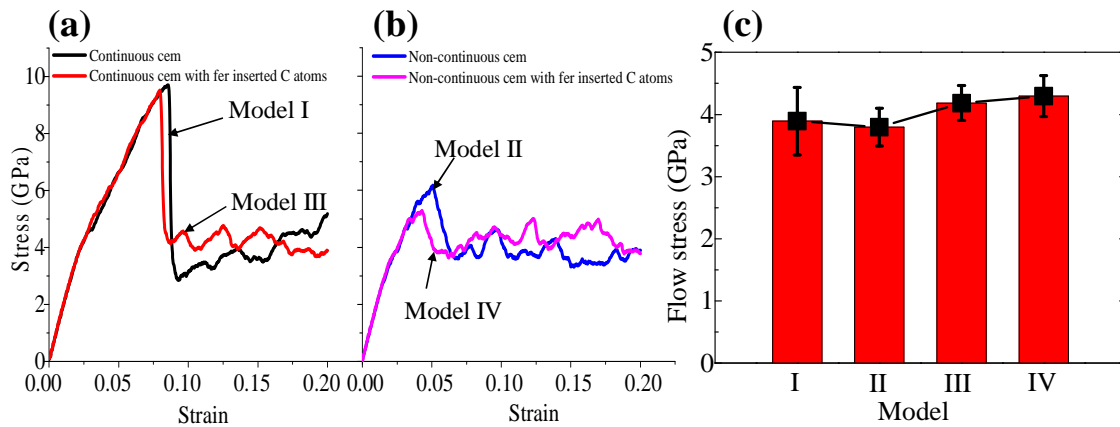


Fig. 12. The stress-strain curves and the calculated flow stresses of four different models under uniaxial tensile loading. (a) The stress-strain curves of the continuous cementite and the continuous cementite with carbon atoms. (b) The stress-strain curves of the non-continuous cementite and the non-continuous cementite with carbon atoms. (c) The calculated flow stresses of the four models.

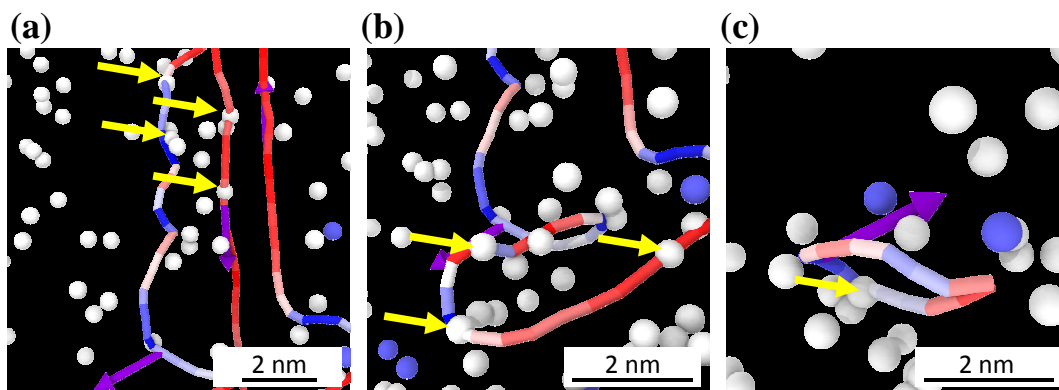


Fig. 13. MD snapshots showing the interaction between dislocations and carbon atoms during plastic flow. (a) and (b) Mobile dislocations are blocked by the carbon atoms. Yellow arrows point to the positions where dislocation fragments are pinned by carbon atoms. (c) A dislocation loop is pinned by carbon atoms. The dislocations lines are extracted by the DXA algorithm. Red, blue and colors between denote screw, edge, and mixed dislocations, respectively. Purple arrows show the Burgers vectors. For a clear vision, all the Fe atoms have been removed and the diameter of

carbon atoms have been enlarged for three times. White and blue balls correspond to the interstitial and substitutional carbon atoms in BCC Fe.

The above discussion has demonstrated that carbon atoms can increase the strength, and we now discuss that the non-continuous cementite layer can increase ductility of pearlite steel. As we know, ferrite is ductile, while cementite is brittle. Spheroidization of cementite leads to non-continuous cementite layers and provides the material with a continuous ferrite matrix, and the material shows more ductility. Fig. 14 shows the snapshots and the associated dislocation configurations by DXA analysis. According to the snapshots of the continuous cementite in Figs. 14a and c, the dislocations were restricted inside ferrite and cannot pass through the cementite into neighboring pure ferrite (without dislocations). Only newly nucleated dislocations were observed after yielding. It is a brittle mechanism since the dislocations may be piled up at the interface and leads to subsequent stress concentration on the interface. On the contrary, the snapshots of the non-continuous cementite models (as shown in Figs. 14b, d) show that the exiting dislocations are easy to spread from discontinuities of cementite into pure ferrite. This means that non-continuous cementite structure contributes to the spread of dislocations and the material behaves more ductile.

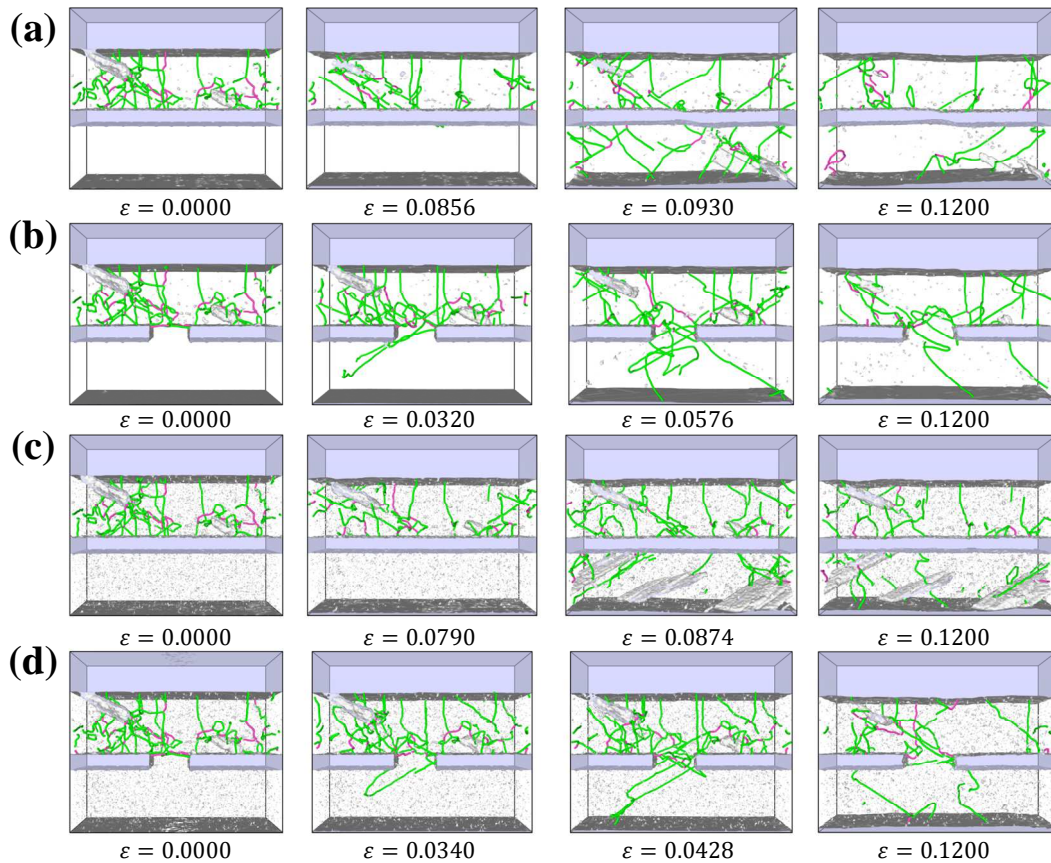


Fig. 14. The snapshots and the associated dislocation pattern by DXA of the four different configurations. From up to bottom, (a), (b), (c), and (d) refer to Model I, Model II, Model III, and Model IV, respectively. From left to right, the snapshots at different strain and rendered of each configuration by using the DXA analysis tool in OVITO. Perfect Fe atoms are not shown in the snapshots for clarity. Green and pink lines are referred to $1/2 \langle 111 \rangle$ and $\langle 100 \rangle$ dislocations, respectively. Gray spots, top gray slab and middle gray slab represent carbon atoms, vacuum and cementite, respectively.

5. Transformation of carbon state

Fig. 15 gives a sketch of microstructures of the as-drawn wires and the annealed wires treated at 325°C for 10 min, which have a greatly improved ductility without

losing their strengths. In the as-drawn state, the wires keep the lamellae structure. A few cementite layers have broken due to the decomposition of cementite and the carbon atoms from the decomposed cementite have migrated into the ferrite. In contrast, the cementite layers of the annealed wires have become disconnected and been separated by the recrystallized cementite particles (Fig. 11). Meanwhile the concentration of carbon in ferrite increases due to decomposition of cementite during the low temperature annealing. As aforementioned, the enhanced solid solution by carbon atoms in ferrite holds the strength of the wires and the improvement of the ductility of wires is from the connecting of adjacent ferrite layers, which releases dislocation pileup on the interface and makes the axial tension of the pearlitic lamellae much easier.

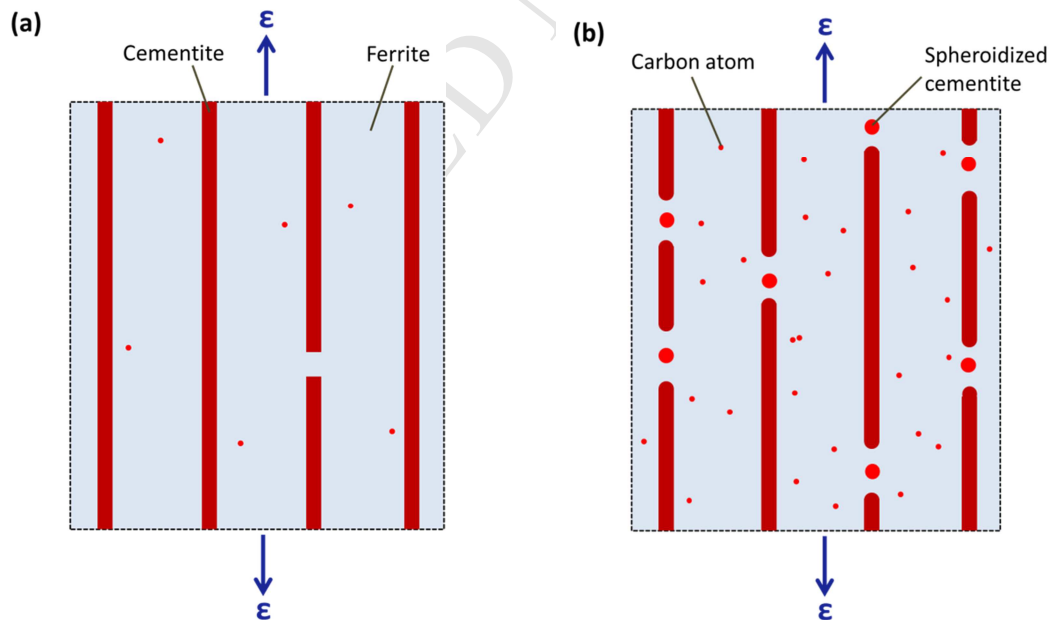
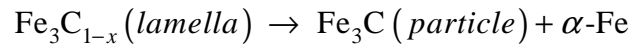


Fig. 15. Schematic diagram showing the microstructure of wires with (a) no annealing, (b) annealing at 325°C for 10 min.

The microstructure and mechanical property of wires are greatly related to the state of carbon atoms. Generally carbons in pearlite wires mainly exist in three forms: the partly dissociated cementite lamella, segregated at dislocations in ferrite via solid solution and the spheroidized grains of recrystallized cementite. APT results have proved the cementite dissolution upon cold drawing and the carbon concentrate in cementite lamellae is lower than 25 at.% (6.7 wt%) for the strict θ -Fe₃C crystals [5, 21, 48]. It is concluded that cementite should be regarded as an interstitial phase Fe₃C_{1-x} with a wide homogeneity range $x = 0 - 0.5$ [49, 50]. Some other reports of cementite deviating from the perfect Fe₃C composition do exist, such as $x = 0.003 - 0.009$ [51], $x = 0.02$ [52], or reach up to $x = 0.25$ [53]. For cold-drawn pearlitic wires, the smaller interlamellar spacing seems to result in higher decomposition of cementite (i.e. the lower carbon content in cementite layers) [5, 54, 55]. Also, as aforementioned, the cementite lamella tends to fragment into multi-grain structure [44, 56], or further turn to amorphization [57, 58] with the increasing of drawing strain. So the partly dissociated cementite layer becomes unstable when temperature is applied on it.

When annealed at a low temperature (175-325°C in this paper), the cementite dissociation continues and carbon atoms partially migrate into ferrite layers to enhance the solid solution effect. As a result, strength of wires is improved but the ductility is decreased. On the other hand, the cementite recrystallization starts to appear along the initial cementite lamella when the temperature rise up to 325°C, which forms perfect Fe₃C grains and the nearby sections are lack of carbon and

could translate into ferrite bcc lattices (Fig. 10). So one have



Then the initial separated ferrite layers can be connected by the newly formed $\alpha\text{-Fe}$ and the ductility of wires is increased rapidly while the wire strength is reduced. With higher temperature, the coarsening of ferrite and cementite grains and the annihilation of dislocations enhance this variation of wire mechanical properties. In summary, annealing at 325°C for 10-30 min is a balanced condition that can greatly improve the wire ductility without losing its strength. From the TEM observation in Figs. 8a and b, the size of spheroidized cementite particles may be a critical condition to reach the status, i.e. the cementite recrystallization grains should be controlled within several nanometers, not more than the thickness of the cementite layer.

Not all the cold-drawn wires can obtain a considerably improved ductility without losing their strengths through annealing. It seems that the drawing extent before heat treatment may play an important role. The wires with drawing strains of 6 [42] and 5 [15] can keep their strengths until the annealing temperature is beyond 150°C and 200°C, respectively. No obvious improvement of strength is found during their annealing while the strength enhancing begin to appear when the drawing strain drops to 4.63 [11]. The temperature under which the strength falls to below that of the as-drawn state exceeds 400°C for wires drawn to 1.7-1.9 [59, 60]. We can conclude that the wire capacity to keep its strength drops with the larger drawing strain and strength improvement could disappear when the strain reaches a relatively severe extent. This may be due to the saturation of carbon in ferrite with highly dissociated

cementite lamellae in heavily drawn wires [21, 61], which makes the further solid solution upon annealing improbable for ferrite [4]. So a moderately drawn wire may be preferable to achieve a balance of strength and ductility, otherwise the strength will be reduced even though the ductility is improved.

At last, the mechanism of cementite decomposition is discussed. Many researchers attribute it to the effect of dislocations [21, 45], even though whether dislocations cut cementite and drag carbon out or dislocations located near the ferrite-cementite interfaces attract carbon is not clear [4]. An atomistic simulation which calculates the energetic profile of carbon binding and migration around a screw dislocation in bcc iron supports the dislocation drag concept by which mobile dislocations can collect and transport carbon within their cores from the cementite into the adjacent ferrite phase [20]. In this paper, the cementite lamellae is deduced to decompose at low temperature annealing, which coincides with the APT results in Ref. [11]. Though it is found that cementite decomposition proceeds during aging after drawing, not during the drawing process [11, 62], dislocations still play an important part in our opinion. On the one hand, high density of dislocations are introduced in ferrite by heavy drawing and the binding energy of carbon to dislocations is greater than that to cementite [46]. On the other hand, dislocations pinning at the ferrite/cementite interfaces enhance the instability of cementite lamella by making it polycrystalline or amorphous [45]. So the active carbon atoms can be attracted to the dislocation locations during low temperature aging. As the dislocation density of wires drops during annealing, the dislocation drag mechanism may be not prevailing. In contrast,

the pipe diffusion mechanism may be dominant. That is dislocations located in the ferrite/cementite interfaces act as accelerated paths (i.e., pipes) for carbon diffusion from cementite to the trap sites in ferrite [63]. The paths (dislocations) are introduced during the cold drawn process, but it still needs enough time and energy for the carbons to migrate from cementite lamellae into ferrite. So the carbon concentration in cementite is still larger than 20 at.% after wire drawing [11], since minimal heating occurs during their wet slow drawing and wires are stored at 243 K to prevent room temperature (RT) aging. When temperature rises, the carbon diffusion process is accelerated and thereupon cementite decomposition happens, like the results in [11, 62] and this paper.

6. Conclusions

The tensile properties and microstructure of pearlitic steel wire under different annealing conditions are studied in this work. When annealed at appropriate temperature and time (325°C for about 10-30 min), we get the enhanced wire property, i.e. the ductility of wire is almost tripled without compromising strength. The strengthening and plasticity mechanisms with relation to the transformation of carbon state are examined in details. Accordingly, the following conclusions can be drawn:

- (1) Under relatively low temperature ($\leq 325^\circ\text{C}$), wires can hold their strength through solid solution of carbon atoms from decomposed cementite lamellae which generates during the cold-drawn process. The heating operation may provide enough energy to make carbons migrate from the unstable dissociated cementite

layers to dislocations in ferrite grains.

- (2) When annealed at medium and higher temperature ($\geq 325^\circ\text{C}$), recrystallization cementite grains begin to appear and continuously grow up along the initial cementite layers. The improvement of wire ductility is obtained since cementite recrystallization leads to fragmenting or disappearing of the cementite lamellae which decreases the restriction to the moving of dislocations. Correspondingly the wire strength decreases with the growth of cementite and ferrite grains.
- (3) The appearance of nano-recrystallized cementite grains ($< 10\text{ nm}$) at a medium temperature may be the appropriate condition to get enhanced wire property. For wires heat-treated at 325°C for 10-30 min in this paper, the solid solution strengthening effect still remains and meanwhile the weakening of cementite layers due to cementite recrystallization has started to improve the wire plasticity. Thus a balance of wire strength and ductility requires carefully control of the annealing condition.

Acknowledgments

The work is supported by the National Key Research and Development Program of China (No. 2017YFB0702003), the Strategic Priority Research Program of the Chinese Academy of Sciences (Grant Nos. XDB22040302, XDB22040303), The Natural Science Foundation of China (Grants Nos. 11572324, 11790292), and the Key Research Program of Frontier Sciences (Grant No. QYZDJSSW-JSC011).

References

- [1] Y. Li, D. Raabe, M. Herbig, P.-P. Choi, S. Goto, A. Kostka, H. Yarita, C. Borchers, R. Kirchheim, Segregation stabilizes nanocrystalline bulk steel with near theoretical strength, *Physical review letters* 113(10) (2014) 106104.
- [2] V.M. Schastlivtsev, I.L. Yakovleva, Fine-lamellar pearlite: The first bulk nanomaterial in carbon steel, *Bulletin of the Russian Academy of Sciences: Physics* 79(9) (2015) 1077-1080.
- [3] L. Li, J. Virta, Ultrahigh strength steel wires processed by severe plastic deformation for ultrafine grained microstructure, *Materials Science and Technology* 27(5) (2011) 845-862.
- [4] C. Borchers, R. Kirchheim, Cold-drawn pearlitic steel wires, *Progress in Materials Science* 82 (2016) 405-444.
- [5] M.H. Hong, W.T. Reynolds, T. Tarui, K. Hono, Atom probe and transmission electron microscopy investigations of heavily drawn pearlitic steel wire, *Metallurgical and Materials Transactions A* 30(13) (1999) 717-727.
- [6] F. Fang, X.J. Hu, S.H. Chen, Z.H. Xie, J.Q. Jiang, Revealing microstructural and mechanical characteristics of cold-drawn pearlitic steel wires undergoing simulated galvanization treatment, *Materials Science and Engineering a-Structural Materials Properties Microstructure and Processing* 547 (2012) 51-54.
- [7] X. Zhang, A. Godfrey, X. Huang, N. Hansen, Q. Liu, Microstructure and strengthening mechanisms in cold-drawn pearlitic steel wire, *Acta Materialia* 59(9) (2011) 3422-3430.
- [8] X. Zhang, N. Hansen, A. Godfrey, X. Huang, Dislocation-based plasticity and strengthening mechanisms in sub-20nm lamellar structures in pearlitic steel wire, *Acta Materialia* 114 (2016) 176-183.
- [9] J. Toribio, A. Valiente, Failure analysis of cold drawn eutectoid steel wires for prestressed concrete, *Engineering Failure Analysis* 13(3) (2006) 301-311.
- [10] D. Raabe, P.P. Choi, Y.J. Li, A. Kostka, X. Sauvage, F. Lecouturier, K. Hono, R. Kirchheim, R. Pippin, D. Embury, Metallic composites processed via extreme deformation: Toward the limits of strength in bulk materials, *Mrs Bulletin* 35(12) (2010) 982-991.
- [11] J. Takahashi, M. Kosaka, K. Kawakami, T. Tarui, Change in carbon state by low-temperature aging in heavily drawn pearlitic steel wires, *Acta Materialia* 60(1) (2012) 387-395.
- [12] S.W. Joung, U.G. Kang, S.P. Hong, Y.W. Kim, W.J. Nam, Aging behavior and delamination in cold drawn and post-deformation annealed hyper-eutectoid steel wires, *Materials Science and Engineering: A* 586 (2013) 171-177.
- [13] Y.J. Li, A. Kostka, P. Choi, S. Goto, D. Ponge, R. Kirchheim, D. Raabe, Mechanisms of subgrain coarsening and its effect on the mechanical properties of carbon-supersaturated nanocrystalline hypereutectoid steel, *Acta Materialia* 84 (2015) 110-123.
- [14] Y.J. Li, P. Choi, S. Goto, C. Borchers, D. Raabe, R. Kirchheim, Evolution of strength and microstructure during annealing of heavily cold-drawn 6.30 GPa hypereutectoid pearlitic steel wire, *Acta Materialia* 60(9) (2012) 4005-4016.
- [15] C. Borchers, Y. Chen, M. Deutges, S. Goto, R. Kirchheim, Carbon-defect interaction during recovery and recrystallization of heavily deformed pearlitic steel wires, *Philosophical Magazine Letters* 90(8) (2010) 581-588.
- [16] C. Borchers, A. Lehmborg, M. Deutges, J. Cizpek, R. Kirchheim, Effect of annealing on point

- defect population in cold-drawn pearlitic steel wires, *Scripta Materialia* 86 (2014) 17-19.
- [17] L. Zhou, F. Fang, X. Zhou, Y. Tu, Z. Xie, J. Jiang, Cementite nano-crystallization in cold drawn pearlitic wires instigated by low temperature annealing, *Scripta Materialia* 120 (2016) 5-8.
- [18] L. Zhou, F. Fang, L. Wang, H. Chen, Z. Xie, J. Jiang, Torsion delamination and recrystallized cementite of heavy drawing pearlitic wires after low temperature annealing, *Materials Science & Engineering A* 713 (2018) 52-60.
- [19] E. Clouet, S. Garruchet, H. Nguyen, M. Perez, C.S. Becquart, Dislocation interaction with C in α -Fe: A comparison between atomic simulations and elasticity theory, *Acta Materialia* 56(14) (2008) 3450-3460.
- [20] G.A. Nematollahi, B. Grabowski, D. Raabe, J. Neugebauer, Multiscale description of carbon-supersaturated ferrite in severely drawn pearlitic wires, *Acta Materialia* 111 (2016) 321-334.
- [21] Y.J. Li, P. Choi, C. Borchers, S. Westerkamp, S. Goto, D. Raabe, R. Kirchheim, Atomic-scale mechanisms of deformation-induced cementite decomposition in pearlite, *Acta Materialia* 59(10) (2011) 3965-3977.
- [22] J. Kim, K. Kang, S. Ryu, Characterization of the misfit dislocations at the ferrite/cementite interface in pearlitic steel: An atomistic simulation study, *International Journal of Plasticity* 83 (2016) 302-312.
- [23] Y.T. Zhou, S.J. Zheng, Y.X. Jiang, T.Z. Zhao, Y.J. Wang, X.L. Ma, Atomic structure of the Fe/Fe₃C interface with the Isaichev orientation in pearlite, *Philosophical Magazine* (2017) 1-12.
- [24] T. Ungár, I. Dragomir, Á. Révész, A. Borbély, The contrast factors of dislocations in cubic crystals: the dislocation model of strain anisotropy in practice, *Journal of Applied Crystallography* 32(5) (1999) 992-1002.
- [25] S. Sato, K. Wagatsuma, M. Ishikuro, E.-P. Kwon, H. Tashiro, S. Suzuki, Precise Characterization of Dislocations and Cementite in Pearlitic Steels at Different Drawing Strains Using X-ray Diffraction, *ISIJ International* 53(4) (2013) 673-679.
- [26] J. Chakraborty, M. Ghosh, R. Ranjan, G. Das, D. Das, S. Chandra, X-ray diffraction and Mossbauer spectroscopy studies of cementite dissolution in cold-drawn pearlitic steel, *Philosophical Magazine* 93(36) (2013) 4598-4616.
- [27] S. Sato, T. Shobu, K. Satoh, H. Ogawa, K. Wagatsuma, M. Kumagai, M. Imafuku, H. Tashiro, S. Suzuki, Distribution and Anisotropy of Dislocations in Cold-drawn Pearlitic Steel Wires Analyzed Using Micro-beam X-ray Diffraction, *ISIJ International* 55(7) (2015) 1432-1438.
- [28] D. Zhou, G. Shiflet, Ferrite: Cementite crystallography in pearlite, *Metallurgical and Materials Transactions A* 23(4) (1992) 1259-1269.
- [29] M. Guziewski, S.P. Coleman, C.R. Weinberger, Atomistic investigation into the atomic structure and energetics of the ferrite-cementite interface: The Bagaryatskii orientation, *Acta Materialia* 119 (2016) 184-192.
- [30] M. Guziewski, S.P. Coleman, C.R. Weinberger, Atomistic investigation into the mechanical properties of the ferrite-cementite interface: The Bagaryatskii orientation, *Acta Materialia* (2017).
- [31] S. Plimpton, Fast parallel algorithms for short-range molecular dynamics, *Journal of computational physics* 117(1) (1995) 1-19.
- [32] L.S.I. Liyanage, S.G. Kim, J. Houze, S. Kim, M.A. Tschopp, M.I. Baskes, M.F. Horstemeyer, Structural, elastic, and thermal properties of cementite (Fe₃C) calculated using a modified embedded atom method, *Physical Review B* 89(9) (2014).
- [33] D.J. Hepburn, G.J. Ackland, Metallic-covalent interatomic potential for carbon in iron, *Physical*

Review B 78(16) (2008) 165115.

- [34] W.G. Hoover, Canonical dynamics: equilibrium phase-space distributions, *Physical review A* 31(3) (1985) 1695.
- [35] S. Nosé, A molecular dynamics method for simulations in the canonical ensemble, *Molecular physics* 52(2) (1984) 255-268.
- [36] M. Parrinello, A. Rahman, Polymorphic transitions in single crystals: A new molecular dynamics method, *Journal of Applied physics* 52(12) (1981) 7182-7190.
- [37] C. Borchers, R. Kirchheim, Cold-drawn pearlitic steel wires, *Progress in Materials Science* 82(Supplement C) (2016) 405-444.
- [38] Y. Li, P. Choi, C. Borchers, S. Westerkamp, S. Goto, D. Raabe, R. Kirchheim, Atomic-scale mechanisms of deformation-induced cementite decomposition in pearlite, *Acta Materialia* 59(10) (2011) 3965-3977.
- [39] L. Martínez, R. Andrade, E.G. Birgin, J.M. Martínez, PACKMOL: a package for building initial configurations for molecular dynamics simulations, *Journal of computational chemistry* 30(13) (2009) 2157-2164.
- [40] A. Stukowski, Visualization and analysis of atomistic simulation data with OVITO—the Open Visualization Tool, *Modelling and Simulation in Materials Science and Engineering* 18(1) (2009) 015012.
- [41] A. Stukowski, V.V. Bulatov, A. Arsenlis, Automated identification and indexing of dislocations in crystal interfaces, *Modelling and Simulation in Materials Science and Engineering* 20(8) (2012) 085007.
- [42] Y.J. Li, A. Kostka, P. Choi, S. Goto, D. Ponge, R. Kirchheim, D. Raabe, Mechanisms of subgrain coarsening and its effect on the mechanical properties of carbon-supersaturated nanocrystalline hypereutectoid steel, *Acta Materialia* 84 (2015) 110-123.
- [43] T. Liu, T. Li, X. Liu, TEM and electron diffraction analysis of ω -Fe to cementite transformation in quenched and tempered high carbon steels, *AIP Advances* 9(4) (2019) 045219.
- [44] X. Hu, L. Wang, F. Fang, Z. Ma, Z. Xie, J. Jiang, Origin and mechanism of torsion fracture in cold-drawn pearlitic steel wires, *Journal of Materials Science* 48(16) (2013) 5528-5535.
- [45] F. Fang, Y. Zhao, P. Liu, L. Zhou, X. Hu, X. Zhou, Z. Xie, Deformation of cementite in cold drawn pearlitic steel wire, *Materials Science and Engineering: A* 608 (2014) 11-15.
- [46] V.N. Gridnev, V.G. Gavriluk, I.Y. Dekhtyar, Y.Y. Meshkov, P.S. Nizin, V.G. Prokopenko, Investigation of carbide phase in strained steel by the method of nuclear gamma resonance, *physica status solidi (a)* 14(2) (1972) 689-694.
- [47] K.O. Henriksson, K. Nordlund, Simulations of cementite: An analytical potential for the Fe-C system, *Physical Review B* 79(14) (2009) 144107.
- [48] C.W. Bang, J.B. Seol, Y.S. Yang, C.G. Park, Atomically resolved cementite dissolution governed by the strain state in pearlite steel wires, *Scripta Materialia* 108 (2015) 151-155.
- [49] V.I. Voronin, I.F. Berger, Y.N. Gornostyrev, V.N. Urtsev, A.R. Kuznetsov, A.V. Shmakov, Composition of cementite in the dependence on the temperature. In situ neutron diffraction study and Ab initio calculations, *Jetp Letters* 91(3) (2010) 143-146.
- [50] C. Jiang, S.A. Maloy, S.G. Srinivasan, A computational method to identify interstitial sites in complex materials, *Scripta Materialia* 58(9) (2008) 739-742.
- [51] F.X. Kayser, Y. Sumitomo, On the composition of cementite in equilibrium with ferrite at room temperature, *Journal of Phase Equilibria* 18(5) (1997) 458-464.

- [52] L. Battezzati, M. Baricco, S. Curiotto, Non-stoichiometric cementite by rapid solidification of cast iron, *Acta Materialia* 53(6) (2005) 1849-1856.
- [53] N.I. Medvedeva, L.E. Kar'kina, A.L. Ivanovskii, Electronic structure and magnetic properties of the α and γ phases of iron, their solutions with carbon, and cementite, *Physics of Metals & Metallography* 101(5) (2006) 440-445.
- [54] X. Sauvage, J. Copreaux, F. Danoix, D. Blavette, Atomic-scale observation and modelling of cementite dissolution in heavily deformed pearlitic steels, *Philosophical Magazine a-Physics of Condensed Matter Structure Defects and Mechanical Properties* 80(4) (2000) 781-796.
- [55] W.J. Nam, C.M. Bae, S.J. Oh, S.J. Kwon, Effect of interlamellar spacing on cementite dissolution during wire drawing of pearlitic steel wires, *Scripta Materialia* 42(5) (2000) 457-463.
- [56] J. Park, S.D. Kim, S.P. Hong, S.I. Baik, D.S. Ko, C.Y. Lee, D.L. Lee, Y.W. Kim, Quantitative measurement of cementite dissociation in drawn pearlitic steel, *Materials Science and Engineering: A* 528(15) (2011) 4947-4952.
- [57] S. Goto, R. Kirchheim, T. Al-Kassab, C. Borchers, Application of cold drawn lamellar microstructure for developing ultra-high strength wires, *Transactions of Nonferrous Metals Society of China* 17(6) (2007) 1129-1138.
- [58] C. Borchers, T. Al-Kassab, S. Goto, R. Kirchheim, Partially amorphous nanocomposite obtained from heavily deformed pearlitic steel, *Materials Science and Engineering: A* 502(1-2) (2009) 131-138.
- [59] T.J. Tarui, T. Tashiro, H. Maruyama, N. Hishida, S. Microstructure Control and Strengthening of High-carbon Steel Wires, *Nippon steel technical reports* (2005).
- [60] K. Makii, H. Yaguchi, M. Kaiso, N. Ibaraki, Y. Miyamoto, Y. Oki, Influence of Si on nano sub-structure of cementite lamellae in pearlitic steel wires, *Scripta Materialia* 37(11) (1997) 1753-1759.
- [61] Y.J. Li, P. Choi, C. Borchers, Y.Z. Chen, S. Goto, D. Raabe, R. Kirchheim, Atom probe tomography characterization of heavily cold drawn pearlitic steel wire, *Ultramicroscopy* 111(6) (2011) 628-632.
- [62] N. Maruyama, T. Tarui, H. Tashiro, Atom probe study on the ductility of drawn pearlitic steels, *Scripta Materialia* 46(8) (2002) 599-603.
- [63] X. Sauvage, Y. Ivanisenko, The role of carbon segregation on nanocrystallisation of pearlitic steels processed by severe plastic deformation, *Journal of Materials Science* 42(5) (2006) 1615-1621.